frontiers | Frontiers in Energy Research

ORIGINAL RESEARCH
published: 08 August 2022
doi: 10.3389/fenrg.2022.957971

PV/WT Integrated System Using the Gray Wolf Optimization Technique for Power Quality Improvement

B. Srikanth Goud[1], Ch. Rami Reddy[2], Ch. Naga Sai kalyan[3], Ramanjaneya Reddy Udumula[4], Mohit Bajaj[5,6], Bdereddin Abdul Samad[7], Mokhtar Shouran[7] and Salah Kamel[8]*

[1]Department of Electrical and Electronics Engineering, Anurag University, Ghatkesar, India, [2]Department of Electrical and Electronics Engineering, Malla Reddy Engineering College, Secunderabad, India, [3]Department of Electrical and Electronics Engineering, Vasireddy Venkatadri Institute of Technology, Guntur, India, [4]Department of Electrical and Electronics Engineering, SRM University, Amaravathi, India, [5]Department of Electrical Engineering, Graphic Era University, Dehradun, India, [6]Department of Electrical Engineering, National Institute of Technology, Delhi, India, [7]Wolfson Centre for Magnatics, School of Engineering, Cardif University, Cardiff, United Kingdom, [8]Department of Electrical Engineering, Faculty of Engineering, Aswan University, Aswan, Egypt

This paper presents the integration of renewable energy sources such as photovoltaics, wind, and batteries to the grid. The hybrid shunt active power filter (HSHAPF) is optimized with the Gray wolf optimization (GWO) and fractional order proportional integral controller (FOPI) for harmonic reduction under nonlinear and unbalanced load conditions. With the use of GWO, the parameters of FOPI are tuned, which effectively minimizes the harmonics. The proposed model has effectively compensated the total harmonic distortions when compared with without the filter and with the passive filter, the active power filter with a PI controller, and the GWO-FOPI-based controller. The performance of the proposed controller is tested under nonlinear and unbalanced conditions. The parameters of the FOPI controller are better tuned with the GWO technique. The comparative results reflect the best results of GWO-FOPI-based HSHAPF. The suggested controller is built in the MATLAB/Simulink Platform.

Keywords: hybrid shunt active power filter, Gray wolf optimization, fractional-order PI controller, renewable energy sources, power quality, harmonic compensation

OPEN ACCESS

Edited by:
Hadi Taghavifar,
UiT The Arctic University of Norway, Norway

Reviewed by:
Hamid Taghavifar,
Urmia University, Iran
Mohd Ashraf Ahmad,
Universiti Malaysia Pahang, Malaysia

****Correspondence:***
Bdereddin Abdul Samad
abdulsamadbf@cardiff.ac.uk

Specialty section:
This article was submitted to Process and Energy Systems Engineering, a section of the journal Frontiers in Energy Research

Received: *07 June 2022*
Accepted: *22 June 2022*
Published: *08 August 2022*

Citation:
Goud BS, Rami Reddy C, Naga Sai kalyan C, Udumula RR, Bajaj M, Abdul Samad B, Shouran M and Kamel S (2022) PV/WT Integrated System Using the Gray Wolf Optimization Technique for Power Quality Improvement. Front. Energy Res. 10:957971. doi: 10.3389/fenrg.2022.957971

1 INTRODUCTION

Power quality (PQ) problems that occur in the distribution system occur when using nonlinear loads. With the development in semiconductor technology, the modeling and usage of power electronic devices are increasing on the end-user side (Mosobi et al., 2015). Because of the usage of power electronic devices, they give rise to many problems like a disturbance in reactive power, a poor power factor, harmonic distortion, and so on (Dash et al., 2018). These problems cause severe effects on the distribution system which result in PQ. To mitigate PQ issues, we have many controlling techniques which ensure harmonic-free systems (Hussain et al., 2019). There are mainly two approaches: load

Abbreviations: APF, active power filter; BESS, battery as the energy storing system; CC-VSI, current controlled voltage source inverter; DG, distributing generation; FOPI, fractional order proportional integral; GWO, Gray wolf optimization; HPFC, hybrid power filter compensation; HSHAPF, hybrid shunt active power filter; PCC, point of common coupling; PV, photovoltaic; PWM, pulse width modulation; PQ, power quality; RES, renewable energy sources; THD, total harmonic distortion.

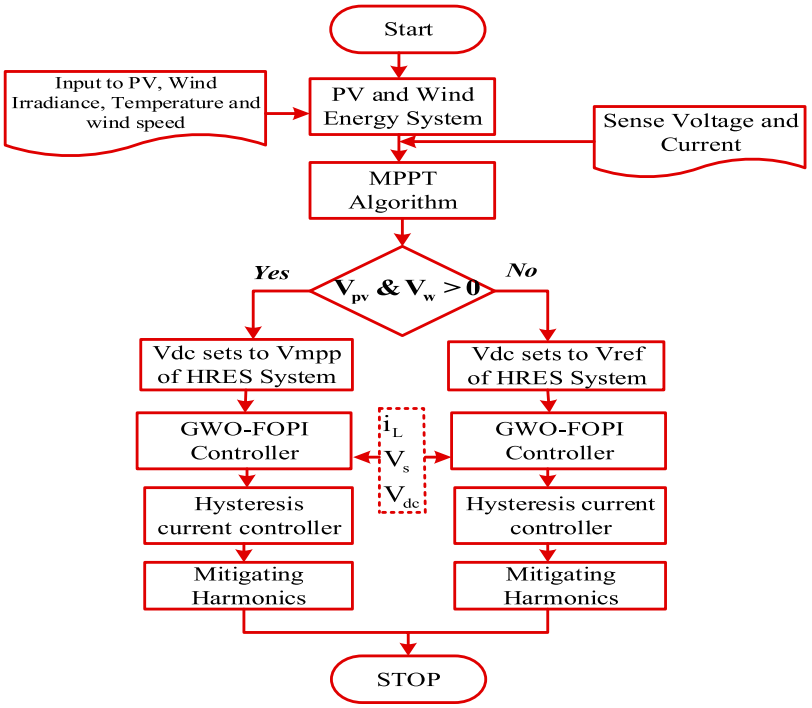

FIGURE 1 | Flow chart of the proposed system.

conditioning and power line conditioning (Amir and Srivastava, 2019). Most of the equipment used nowadays is more sensitive to the adverse effects of PQ problems (Goud and Reddy, 2020).

In this approach, at the point of common coupling (PCC), the proposed approach minimizes the effect produced by nonlinear loads. Initially, passive filter usage was widely considered for harmonic elimination and reactive power compensation. Due to various remarkable disadvantages like constant compensation performance, a large size, resonance, and so on, later on, the usage became less. To mitigate the reactive power compensation and harmonics (Jamil et al., 2019), active power filters (APFs) became more prominent as the performance characteristics are very effective when compared with the conventional filters (Meral and Celik, 2018).

APFs are devices that generally produces an equal quantity of harmonics when compared with the load with a phase shift of 180^0. These harmonics are injected into the linear PCC, and load current harmonics are mitigating and supply becomes sinusoidal (Pang et al., 2019). They are broadly classified as series APF and shunt APF. Shunt APF is used to mitigate the load current harmonics by inserting equal and opposite harmonic compensating current. **Table 1** presents the brief research works carried out in the literature. This literature mainly focuses on grid integration using RES, APFs, PQ issues, and various types of controllers designed to mitigate in the hybrid integrated system.

The designed system is a combination of photovoltaics (PVs), wind, and batteries as energy-storing devices (Arkhangelski et al., 2019). The purpose of using a battery is not only to provide backup but also to store the excess amount of generated energy to meet the demand. **Figure 1** shows the structure of HSHAPF CC-VSI which is grid interfaced through a DC-link capacitor (Naresh et al., 2018; Muthukumar and Balamurugan, 2019; Goud and Rao, 2020; Kuchibhatla et al., 2020). To increase the voltage if required, a step-up transformer is connected to the AC side of the inverter at the PCC. At the PCC, an uncontrolled bridge rectifier nonlinear load is connected. To minimize the load current harmonics, an inverter control is being utilized and transfers the DG power flow to the PCC.

1.1 Primary Aim and Structure of the Paper

In this paper, total harmonic distortion (THD) reduction under nonlinear load and unbalanced load without the filter, with the passive filter, and with APF using a PI controller and the proposed controller is introduced, which results in the best reduction of harmonics under various load conditions.

The following is the paper's primary contribution:

- The DG is the combination of PV, wind, and batteries as storing devices. Energy can be stored in the batteries when an excess amount is generated and can be used to compensate for the required load under various conditions.
- The system is an integrated system. The dynamic performance is observed under various load conditions when connected at the PCC. This integration creates the harmonics, which causes the affect the system's stability
- A metaheuristic algorithm known as the Gray wolf optimization (GWO) technique is introduced, which generates the best optimal pulse for the proposed

TABLE 1 | Review of recent research works.

Contribution	Authors	References
• They designed the PV and wind model with and without APF when connected to the nonlinear load. • They developed a DC-DC boost converter and inverter which convert to AC with the same frequency, amplification, and phase of the grid that will be connected to PV and wind system fundamental elements.	Aljendy et al.	Aljendy et al. (2019)
• They represented the performance, operational concepts, and analysis of D-STATCOM, which is widely used power electronic equipment designed to improve the PQ in low-voltage distribution systems. • They used VSC to improve the PF and THD reduction when LCL passive filters are employed.	E. Rambabu et al.	Rambabu et al. (2011)
• They designed an intelligent controller with SHAPF in the integrated hybrid energy system to mitigate the PQ issues. During the distribution of power, most of the PQ issues are raised due to the nonlinear loads. • Intelligent techniques are developed in the PV, wind, and fuel cell integrated system. Based on neuro-fuzzy system dynamics, pf SHAPF is optimized using adaptive control algorithms.	Ravinder et al.	Ravinder and Bansal, (2019)
• They developed a hybrid renewable energy source system integrated to the grid with UPQC, which is effectively used to mitigate PQ problems such as sag, swell, and disturbances. • They implemented an atom search optimization-based fractional order proportional integral controller.	C. R. Reddy et al.	Reddy et al. (2021)
• They proposed a microgrid power system that is boosted with a dual-voltage source inverter. • It mainly consists of two inverters for enabling the grid to exchange power produced by RES and offset the nonlinear load and unbalanced loads. • One inverter reduces the cost by implementing the filter voltage and increasing the usage of microgrid power, and the other inverter reduces the DC link voltage.	N. Kumar et al.	Bhupesh et al. (2019)
• They proposed a three-phase SHAPF nonlinear control approach. This design minimized the reactive, harmonic current components and unbalances. • To mitigate the disturbances of the conventional method, they proposed a conventional delay compensation approach which produces reference current with less precise delays. • Synchronous reference frame theory is used in the first stage to remove reference currents from nonlinear loads to compensate for the delay; a three-phase R-L loaded diode rectifier is used.	Rahmani S et al.	Rahmani et al. (2010)
• The proposed fast load voltage control and efficient voltage mitigation using a PWM voltage source inverter (VSI). • The control approach is designed based on a hybrid linear with a voltage controller for variable structure control and a dead bear controller. • The proposed system is used to balance voltage at PCC with VSI-based DG.	Mohamed et al.	Mohamed and El-Saadany, (2009)
• They designed a VSC-based hybrid power filter compensator (HPFC) for mitigating the harmonics and reactive power compensation in wind energy-based DG systems. • The multi-loop dynamic error control unit is designed with a DC voltage tracking loop to ensure robust and rapid control over the HPFC.	Imam et al.	Imam et al. (2020)
• They proposed UPQC and mainly focused on the distribution network problems such as reducing losses, voltage drop, overloads, and unbalance in line currents. • To improve the reliability, reduce losses, and increase the voltage profile, UPQC with reliability indices has been designed.	Dashtdar et al.	Dashtdar et al. (2021a)
• To meet the PQ requirements and mitigate them, they designed reliable power filters. They discussed SHAPF with the conventional PI controller to regulate DC link voltage and PQ enhancement. • For reference current extraction, instantaneous eference frame theory is used. To obtain gate pulses, hysteresis current control is used to generate the gate pulses to the VSI.	A. Sharaf et al.	Sharaf et al. (2010)

fractional order proportional integral (FOPI) controller, which effectively functions to mitigate the PQ issues and reduce THD.

The following sections of the papers are categorized as follows: **Section 2** describes the proposed system and design, **Section 3** proposes the mathematical modeling of the controller, **Section 4** describes the proposed HSHAPF, **Section 5** illustrates the GWO technique and FOPI controller, **Section 6** deals with results and discussion, and **Section 7** is the conclusion.

2 PROPOSED TEST SYSTEM

The proposed modeling is designed using both passive and active filters. The designed model improves the compensation characteristics of the filter, which reduces the disadvantages of both active and passive filters. **Figure 1** represents the flow chart of the proposed system. **Section 2** describes the detailed construction of the system design. In this proposed paper, HSHAPF is implemented with the combination of the LC passive filter and voltage source PWM converter illustrated in **Figure 2**, which illustrates the renewable energy resources (RES) and HSHAPF connected to the grid. **Table 2** illustrates the design parameters. **Figure 3** depicts the basic structure of SHAPF. This design is tested at various loads such as nonlinear loads and unbalanced loads. The characteristics of both filters are designed in providing the best performance under various operating conditions. To filter out the harmonics, the designed structure is modeled with storage systems using the battery, DC link, and switches with antiparallel diodes (Goud and Rao, 2021). At PCC, compensating current is injected using a voltage source converter to mitigate the harmonics. To overcome the power rating required for the PWM converter, the system is modeled using both active and passive filters to mitigate the harmonics. Here, power MOSFETs are used in

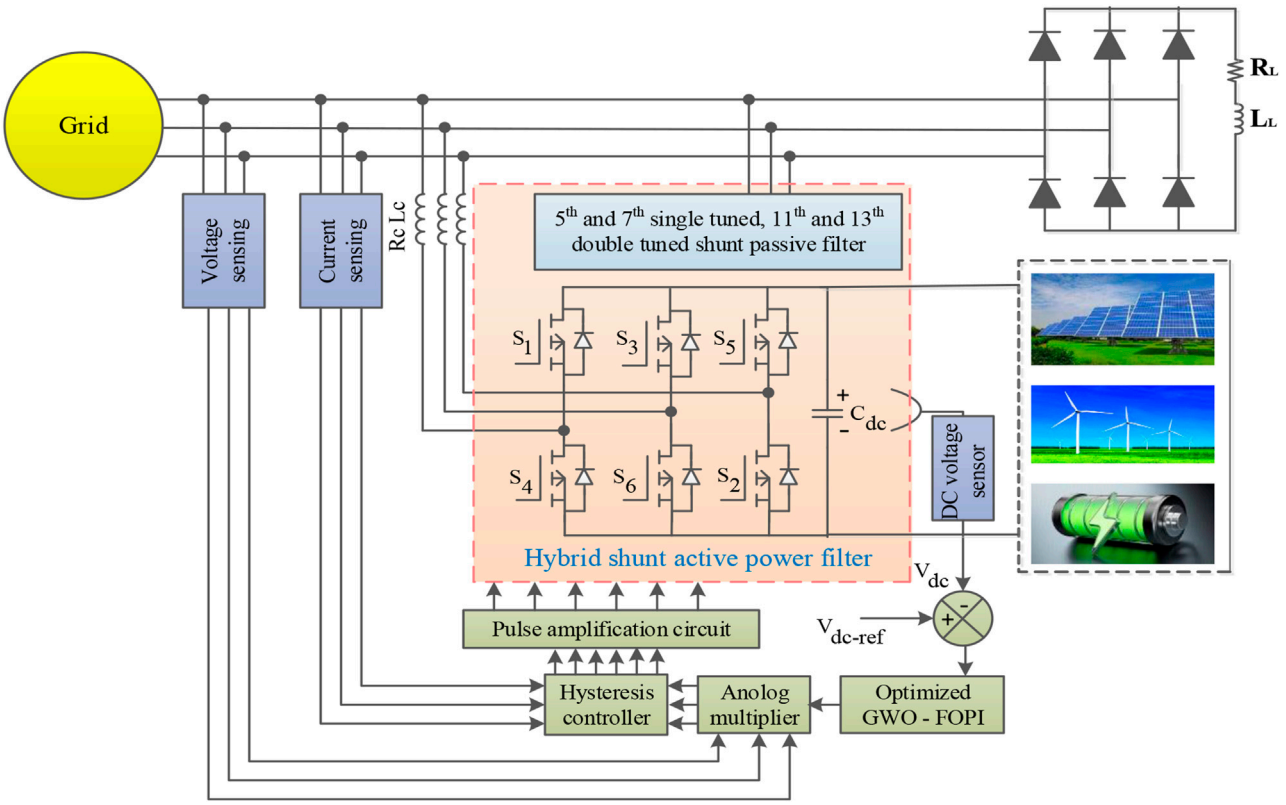

FIGURE 2 | Schematic diagram of RES-based HSHAPF.

TABLE 2 | System parameters.

S.No	Description	Parameters	Values
1		Voltage source	230 V
		Frequency	50 Hz
2	PV	Irradiance	1000
3		Diode resistance	595.5 Ω
4		Forward voltage	0.8 V
6	Wind	Base wind speed	12 m/s
7		Base rotational speed	0.4 m/s
8		Stator phase resistance	1.5 Ω
9		Armature inductance	8.5e-3H
10	Battery	Type	Nickel-metal-hydride
		The initial state of charge	100
11	Load	Nominal voltage	230 V

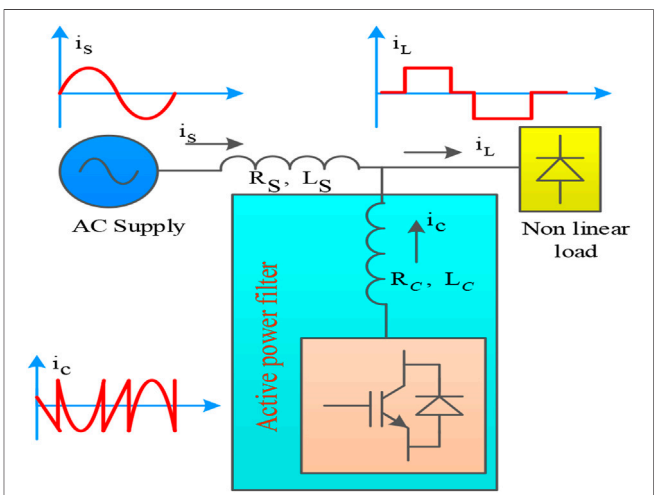

FIGURE 3 | Basic structure of shunt APF.

designing the PWM converters, which is cost-effective. To eliminate the harmonic at the PCC, equal and opposite magnitude harmonic current has to be injected, which also improves the PQ in the distribution system.

2.1 Equivalent Circuit of the Photovoltaic

The structure of PV is depicted in **Figure 4**, whose panel terminal current and voltage are computed based on the below equation (Mosobi et al., 2015; Dash et al., 2018)

$$I_p = I_{sc} - I_o\left\{\exp\left[\frac{Q}{akt}\left(V_p + I_p R_{SE}\right) - 1\right]\right\} - \frac{V_p + I_{sc}R_{se}}{R_{sh}} \quad (1)$$

$$V_p = \frac{akt}{Q}\ln\left\{\frac{I_{sc}}{I_p} + 1\right\} \quad (2)$$

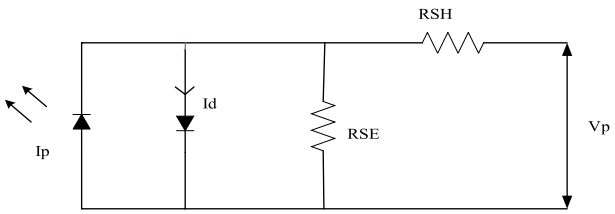

FIGURE 4 | Schematic diagram of PV.

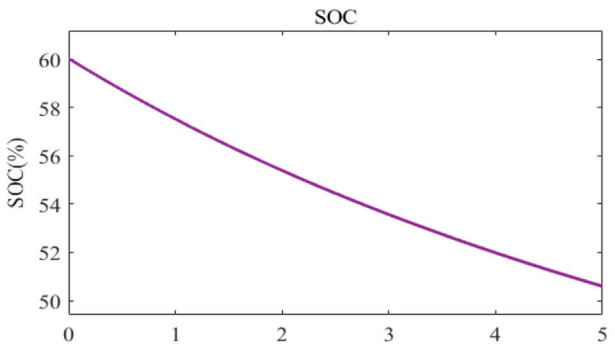

FIGURE 5 | Performance of the battery under the SOC.

where k is Boltzmann's constant, Q is the electron charge, a is the diode ideality factor, R_{SE} is the series resistance, t is the temperature in Kelvin, R_{SH} is the shunt resistance, V_P is the voltage of the cell, and I_{Sc} is the current. The power of a PV panel is described as follows:

$$P_{PV}(t) = N_{pv}(t) \times I_{pv}(t) \times V_{pv}(t) \tag{3}$$

where $N_{pv}(t)$ are several cells in the PV array, $P_{pv}(t)$ is the power of PV, $V_{pv}(t)$ $V_{pv}(t)$ is the voltage of PV, and $I_{pv}(t)$ is the current of PV. Maximum power extraction from the grid does not occur at any time as it is concerned with the allocation of current and load. MPPT is a standard method for capturing the maximum power from PV under load. There are many other sorts of methods; in this case, perturb and observer approaches are applied.

2.2 Modeling of the Wind Turbine

The wind turbine (WT) generates the output power, which was determined by wind speed as well as the hub's height. The WT is reliant on wind speed, which is calculated using the below equation (Amir and Srivastava, 2019)

$$P_{wind} = \begin{cases} 0 \\ P_R \bullet \dfrac{v - v_c}{v_R - v_c} \text{for} (V_c \le v \le v_R) \\ P_R \text{for} \left(V_R \le v \le v_f \right) \end{cases} \tag{4}$$

where P_R is the electrical power rating, v_C is the decrease in wind speed, v_R is the wind speed predicted, and v_F is the wind speed cut off. The impacts of WT installation height must be taken into account while calculating WT performance.

2.3 Modeling of the Battery as an Energy Storing System

The battery size is computed and developed using the reference autonomy day in the event of a required power requirement (AD) shown in the below equation (Goud and Reddy, 2020)

$$B^{capacity} = \frac{\text{Autonomyday} \times P^L}{\eta^I * \eta^B * \text{DOD}} \tag{5}$$

where η^B is the efficiency of the battery, DOD is the depth of discharge rate of the battery, P^L is the demand power, and η^I is the inverter efficiency. The amount of time a battery can produce electricity to meet load demand is described as AD. When RES generates excess electricity, it is used to charge a battery in the HRES system. The following equation is used to calculate battery power

$$B^P = P_{PV}(t) + P_{WT}(t) - \frac{P_L(t)}{\eta^I} \tag{6}$$

where B^P is the battery power. In the battery, $P_L(t)$ is the load demand of the system. As stated below, state of charge (SOC) is a critical parameter in HRES that is linked to additional energy creation and energy shortage. **Figure 5** depicts SOC

$$SOC(t) = \begin{Bmatrix} SOC(t-1)(1-\mu) + \\ \left(P_{pv}(t) + P_{WT}(t) - \dfrac{P_L(t)}{\eta^I} \right) \times \\ \eta^B, P_{pv}(t) + P_{WT}(t) > P_L(t) \\ SOC(t-1)(1-\mu) + \\ \left(\dfrac{P_L(t)}{\eta^I} - P_{pv}(t) + P_{WT}(t) \right) \times \\ \eta^B, P_{pv}(t) + P_{WT}(t) < P_L(t) \end{Bmatrix} \tag{7}$$

where μ is the battery self-discharge rate.

3 MATHEMATICAL MODELING OF THE PROPOSED SYSTEM

A set of n harmonics with n = {1,2,3,. . ..N} is proposed. At the same position, components are found, and they are current I_L (t) and Voltage V_s (t), which can be expressed as the equation that follows (Pang et al., 2019 and Aljendy et al., 2019). **Figures 6**, **7** depict the mathematical modeling of the controller

$$V_s(t) = \begin{bmatrix} V_{s1} \\ V_{s2} \\ V_{s3} \end{bmatrix} = \begin{bmatrix} \sum_{n=1}^{N} V_{sn1} \sin(n(\omega t)) \\ \sum_{n=1}^{N} V_{sn2} \sin\left(n\left(\omega t - 120^0\right)\right) \\ \sum_{n=1}^{N} V_{sn3} \sin\left(n\left(\omega t - 240^0\right)\right) \end{bmatrix} \tag{8}$$

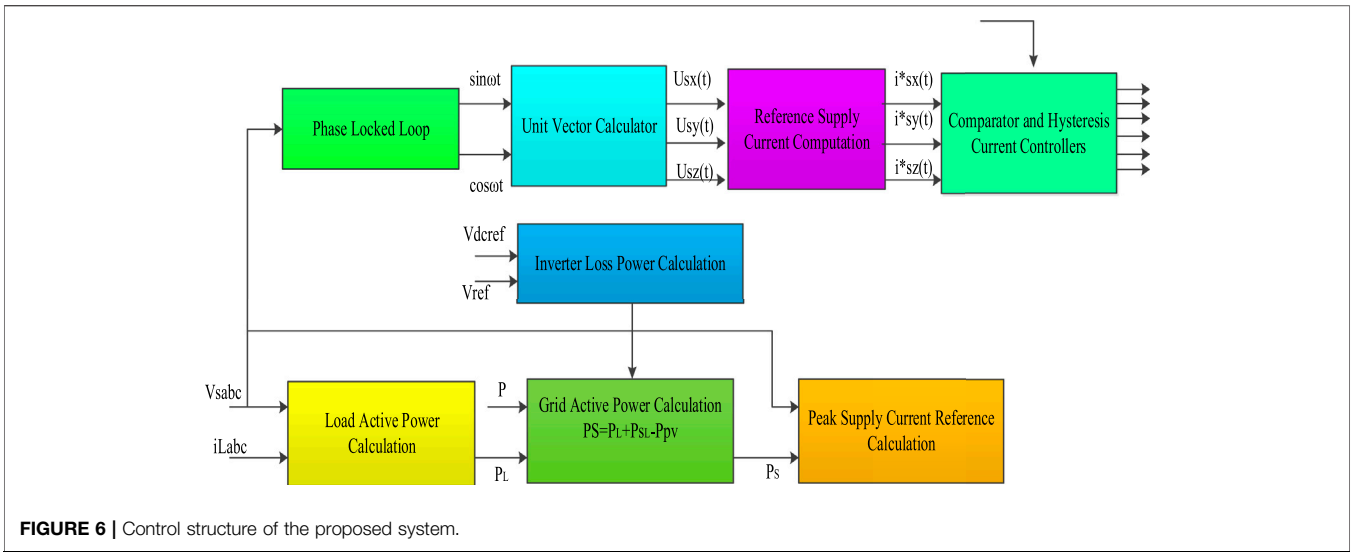

FIGURE 6 | Control structure of the proposed system.

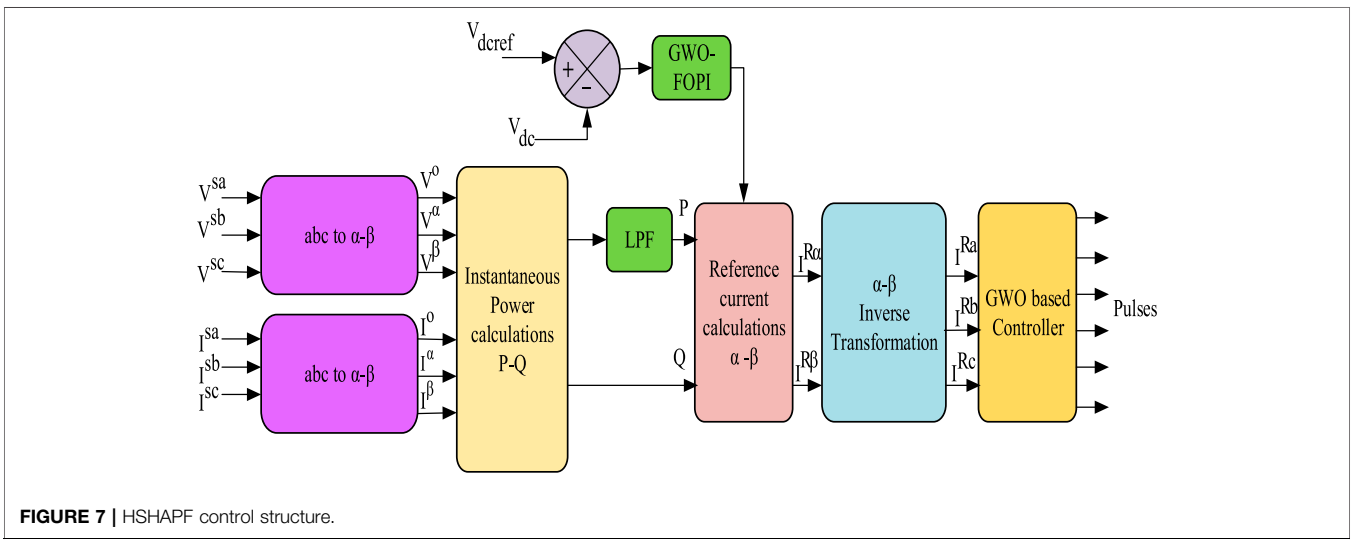

FIGURE 7 | HSHAPF control structure.

$$i_L(t) = \begin{bmatrix} i_{l1} \\ i_{l2} \\ i_{l3} \end{bmatrix} = \begin{bmatrix} \sum_{n=1}^{N} I_{Ln1} \sin\left(n\omega t - \phi_{n1}\right) \\ \sum_{n=1}^{N} I_{Ln2} \sin\left(n\left(\omega t - 120^0\right) - \phi_{n2}\right) \\ \sum_{n=1}^{N} I_{Ln3} \sin\left(n\left(\omega t + 120^0\right) - \phi_{n3}\right) \end{bmatrix} \quad (9)$$

(I_{Ln1}, I_{Ln2}, I_{Ln3}) are load current peak values; (V_{sn1}, V_{sn2}, V_{sn3}) are PCC voltage peak values; and ϕ_{n1}, ϕ_{n2}, and ϕ_{n3} are harmonic component phase angles of the nth order.

The real power delivered by the grid P_s should be similar to the grid power provided for compensating at a high power factor using the below equation (Aljendy et al., 2019)

$$P_s = P_L + P_l - P = \frac{3}{2} V_{s1} I_{s1}^{*} \quad (10)$$

where the real loss of power is P_l, the actual power delivered by the RES is P, and the real power of the load is P_L; as a result, the maximum value of the basic aspect of typical point voltage is a key component, and Is* is an essential component and is the source current component expressed in the below equation (Ravinder and Bansal, 2019)

$$I_{s1}^{*} = \frac{2P_s}{3V_{s1}} \quad (11)$$

$$\begin{aligned} I_{sx}^{*}(t) &= I_{s1}^{*} u_{sx} \\ I_{sy}^{*}(t) &= I_{s1}^{*} u_{sy} \\ I_{sz}^{*}(t) &= I_{s1}^{*} u_{sz} \end{aligned} \quad (12)$$

$$\begin{aligned} u_{sx}(t) &= u_a(t) \\ u_{sy}(t) &= -\frac{1}{2} u_a(t) + \frac{\sqrt{3}}{2} u_b(t) \\ u_{sz}(t) &= -\frac{1}{2} u_a(t) - \frac{\sqrt{3}}{2} u_b(t) \end{aligned} \quad (13)$$

where $u_a(t) = \sin\omega t$ and $u_b(t) = \cos\omega t$ as expressed by the equations (Bhupesh et al., 2019; Reddy et al., 2021) indicate the

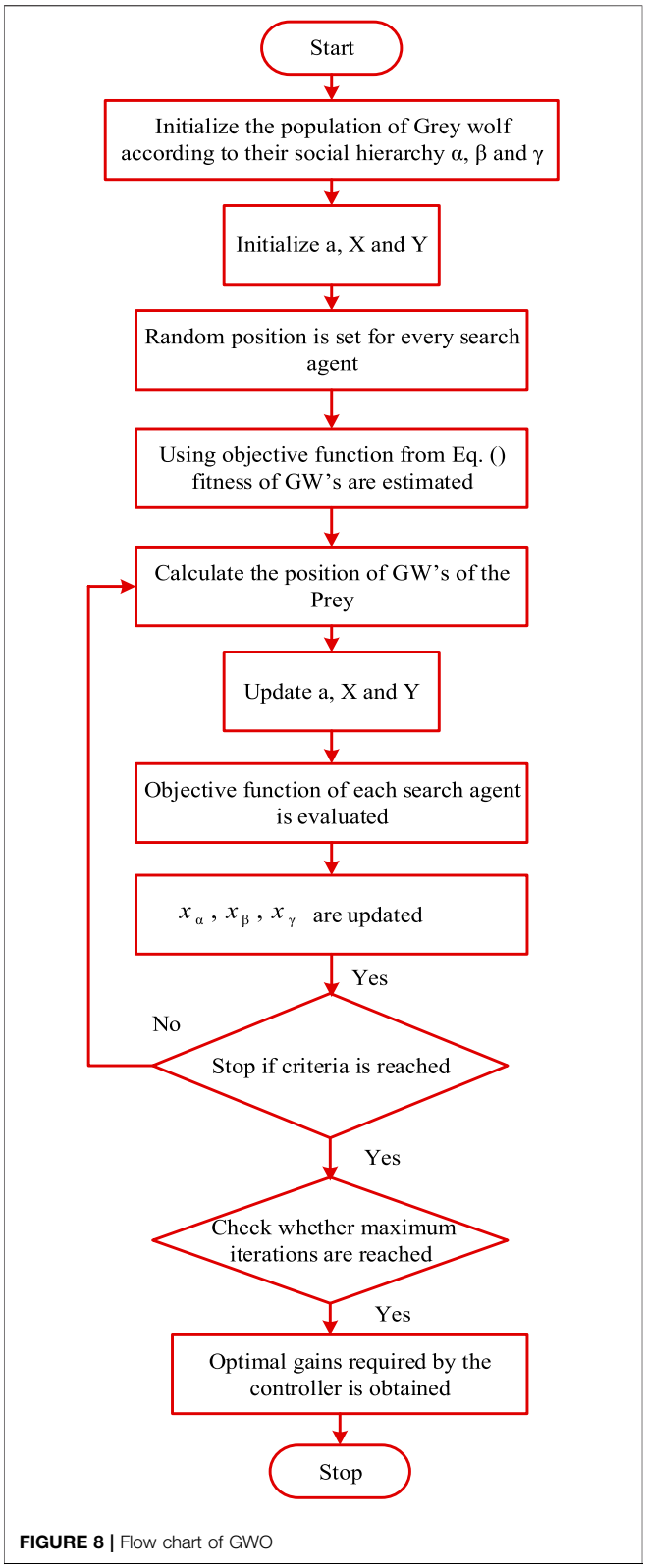

FIGURE 8 | Flow chart of GWO

distance between adjacent reference currents. The current inverter and standard inverter current errors are sent to the HCC ($\Delta ic_a, \Delta ic_b, \Delta ic_c$), which adjusts the duty ratio of the

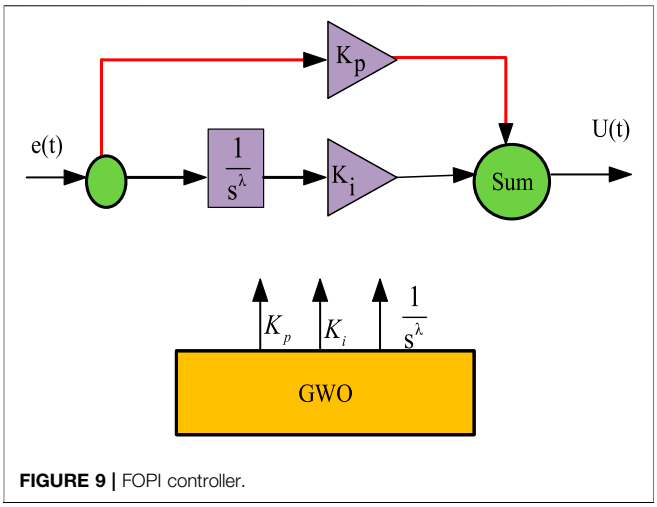

FIGURE 9 | FOPI controller.

PWM inverter expressed in the below equation (Rahmani et al., 2010)

$$\begin{aligned}\Delta i_{ca} &= I^*_{c1}(t) - i_{c1}\\ \Delta i_{cb} &= I^*_{c2}(t) - i_{c2}\\ \Delta i_{cc} &= I^*_{c3}(t) - i_{c3}\end{aligned} \tag{14}$$

Determined by the difference between the real and perceived currents of the inverter, the hysteresis regulator regulates and modulates pulse in both gate actuators of a grid-connected adapter. In phase A of the inverter, the S_1 switch is on, while $\Delta_{ic1} > H_b$ and S4 are off, and vice versa if $\Delta_{ic1} < H_b$.H_b the hysteresis band's width. The period of the switching pulses for either leg will be the same.

4 HYBRID SHUNT ACTIVE POWER FILTER CONTROL STRUCTURE

The p-q theory is used, which is mainly based on a-b-c conversion into α-β-0 coordinates and α-β-0 conversation into a-b-c parameters, which are familiarly known as Clark's transformation and inverse transformation, respectively (Durairasan and Balasubramanian, 2020; Hari Prabhu and Sundararaju, 2020; Sureshkumar and Ponnusamy, 2020). The transformation is shown in **Figures 6**, **7**, from which compensating currents are generated.

In this transformation, three-phase source voltage and load current are converted to stationary reference frame α-β-0 using the below equations (Mohamed and El-Saadany, 2009; Imam et al., 2020)

$$\begin{bmatrix} V^{s0} \\ V^{s\alpha} \\ V^{s\beta} \end{bmatrix} = \sqrt{\frac{2}{3}} \begin{bmatrix} \frac{1}{\sqrt{2}} & \frac{1}{\sqrt{2}} & \frac{1}{\sqrt{2}} \\ 1 & -\frac{1}{2} & -\frac{1}{2} \\ 0 & \frac{\sqrt{3}}{2} & -\frac{\sqrt{3}}{2} \end{bmatrix} \begin{bmatrix} V^{sa} \\ V^{sb} \\ V^{sc} \end{bmatrix} \tag{15}$$

TABLE 3 | FOPI controller parameters.

Parameter	Value
Search agents	50
No of iterations	10
Dim	3
K_p	5.9537
K_i	11.1470
λ	0.8798

$$\begin{bmatrix} I^{l0} \\ I^{l\alpha} \\ I^{l\beta} \end{bmatrix} = \sqrt{\frac{2}{3}} \begin{bmatrix} \frac{1}{\sqrt{2}} & \frac{1}{\sqrt{2}} & \frac{1}{\sqrt{2}} \\ 1 & -\frac{1}{2} & -\frac{1}{2} \\ 0 & \frac{\sqrt{3}}{2} & -\frac{\sqrt{3}}{2} \end{bmatrix} \begin{bmatrix} I^{La} \\ I^{Lb} \\ I^{Lc} \end{bmatrix} \tag{16}$$

where $I^{l\alpha}$ and $I^{l\beta}$ are phase-neutral currents, while I^{La}, I^{Lb}, and I^{Lc} are three-phase load currents. Three-phase supply voltages are V^{Sa}, V^{Sb}, and V^{Sc}, whereas the phase-neutral voltages are $V^{S\alpha}$, $V^{S\beta}$. The instantaneous values of actual and unconsidered powers are determined using phase neutral voltages and load currents (Hari Prabhu and Sundararaju, 2020; Sureshkumar and Ponnusamy, 2020). In the shunt active filter, the actual and reactive power is determined using the below equation (Dashtdar et al., 2021a)

$$\begin{bmatrix} P \\ Q \end{bmatrix} = \begin{bmatrix} V^{s\alpha} & V^{s\beta} \\ -V^{s\beta} & V^{s\alpha} \end{bmatrix} \begin{bmatrix} I^{l\alpha} \\ I^{l\beta} \end{bmatrix} \tag{17}$$

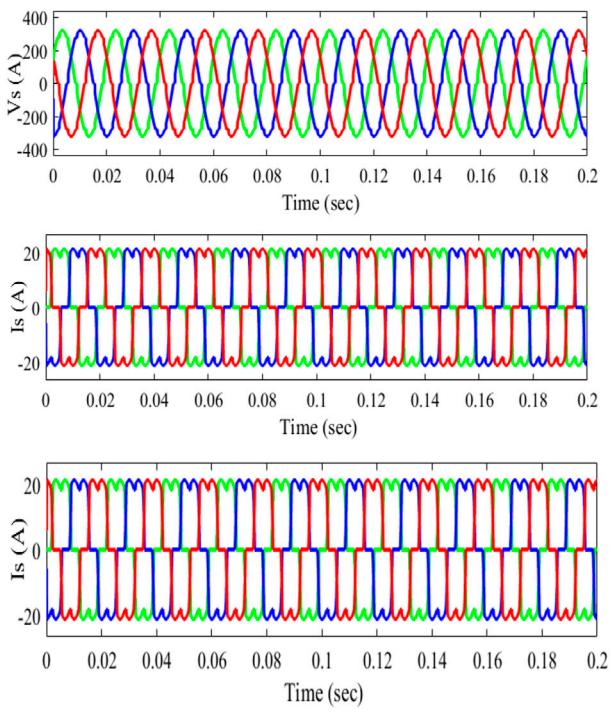

FIGURE 10 | Without the filter for nonlinear load source voltage (V_s), source current (I_s), and load current (I_L).

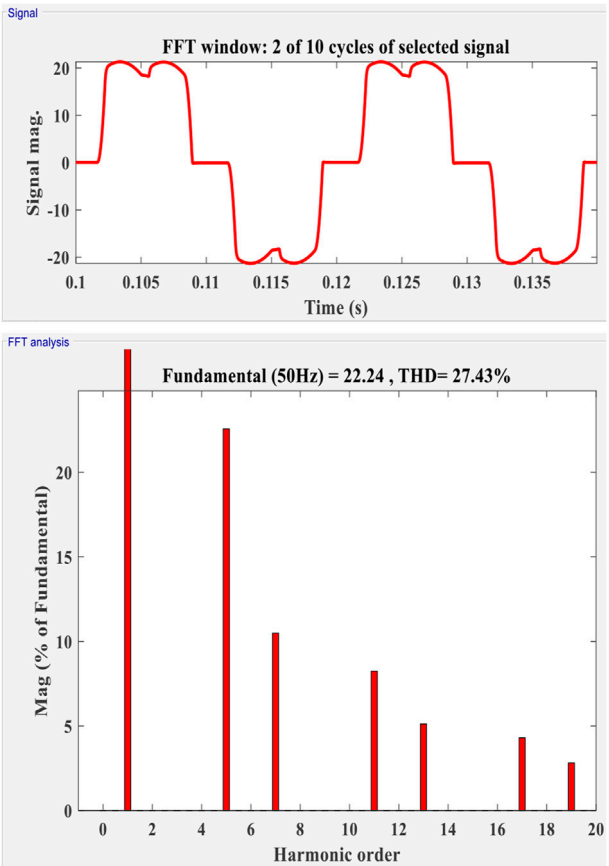

FIGURE 11 | Without the filter for unbalanced load source voltage (V_s), source current (I_s), and load current (I_L).

Using the below equation (Sharaf et al., 2010), the reference currents are evaluated

$$\begin{bmatrix} I^{Ra} \\ I^{Rb} \\ I^{Rc} \end{bmatrix} = \sqrt{\frac{2}{3}} \begin{bmatrix} 1 & 0 \\ -\frac{1}{2} & \frac{\sqrt{3}}{2} \\ -\frac{1}{2} & -\frac{\sqrt{3}}{2} \end{bmatrix} \begin{bmatrix} I^{R\alpha} \\ I^{R\beta} \end{bmatrix} \tag{18}$$

I^{Ra}, I^{Rb}, and I^{Rc} represent the reference currents of an HSHAPF. The reference current is used to calculate the erroneous current, which must be modified using the GWO-optimized PI controller. Based on system error reduction, the SHAPF creates optimal pulses. The GWO is utilized to compute the optimal solution and the best pulses for adjusting the FOPI controller. The next section describes a detailed description of the recommended strategy as well as a flow chart.

5 GRAY WOLF OPTIMIZATION TECHNIQUE

GWO is new optimization that is supported by the swarm intelligence which is inspired by the psychology of GW to

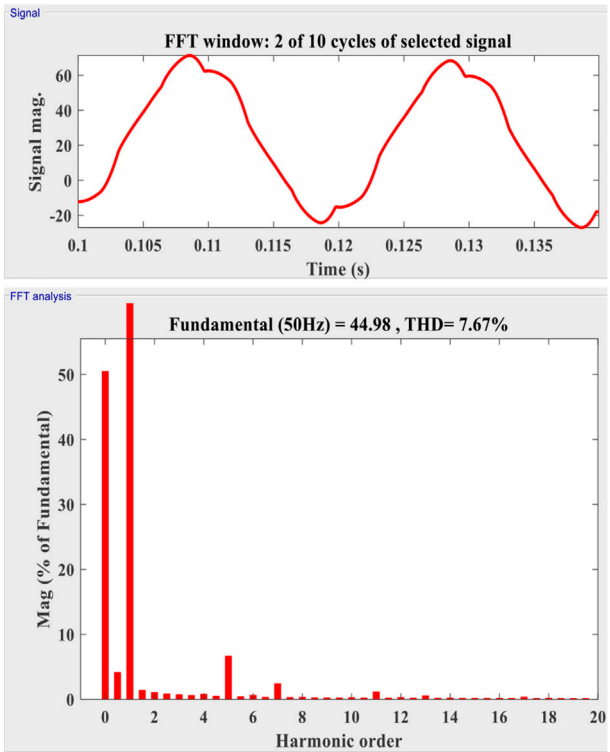

FIGURE 12 | With the passive filter for nonlinear load source voltage (V_s), source current (I_s), and load current (I_L).

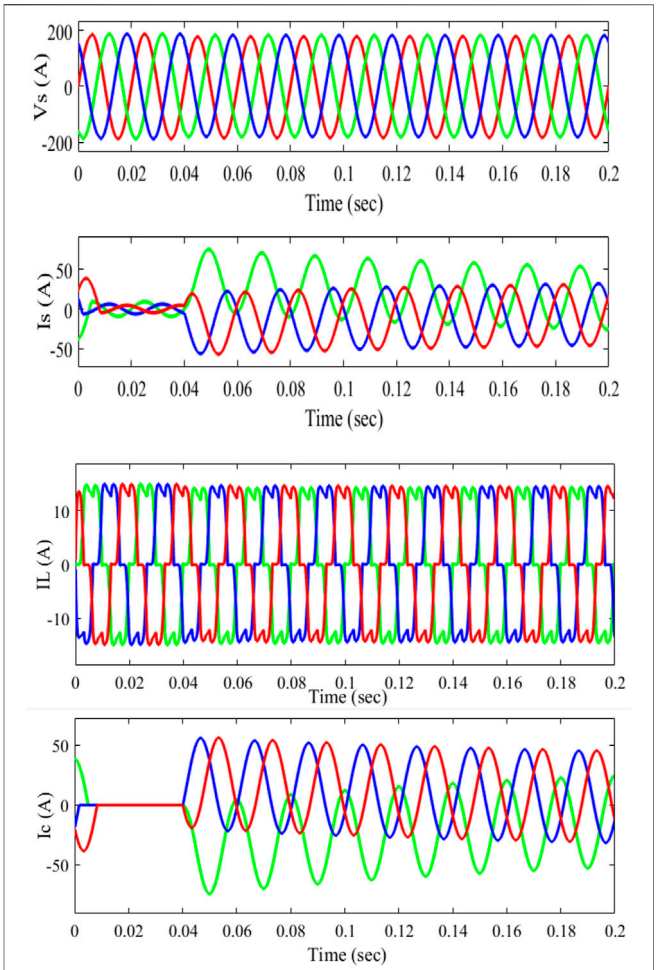

FIGURE 13 | Analysis of PV irradiance, PV power, wind speed, and wind power.

hunt prey illustrated in **Figure 8**. GWs are always in groups and adjusted in a location during the hunting process. To model the hunting procedure mathematically, the optimal best solution is given to the alpha group act following beta and delta packs (Goud et al., 2020). GWs create a kink around the injured to start hunting the prey, generally written as

$$\vec{d} = \left|\vec{c}.\vec{x}_p(t) - \vec{x}(t)\right| \tag{19}$$

$$\vec{x}(t+1) = \left|\vec{x}_p(t) - \vec{a}.\vec{d}\right| \tag{20}$$

't' in **Eq. 19** indicates the current iteration. The vectors x and x_p indicate the GW and the wound location, respectively, and coefficient vectors X and Y are framed from the below equations (Naresh et al., 2018; Goud and Rao, 2020)

$$\vec{X} = 2.\vec{a}.\vec{r}_1 - \vec{a} \tag{21}$$

$$\vec{Y} = 2.\vec{r}_2 \tag{22}$$

r_1 and r_2 indicate the random vector, which varies between (0, 1), while the component "a" falls from 2 to 0 throughout the iteration. Using the below equations (Durairasan and Balasubramanian, 2020; Kuchibhatla et al., 2020; Goud and Rao, 2021), the hunting process is calculated

$$\left.\begin{aligned}\vec{d}_\alpha &= \left|\vec{c}_1.\vec{x}_\alpha - \vec{x}\right| \\ \vec{d}_\beta &= \left|\vec{c}_2.\vec{x}_\beta - \vec{x}\right| \\ \vec{d}_\gamma &= \left|\vec{c}_3.\vec{x}_\gamma - \vec{x}\right|\end{aligned}\right\} \tag{23}$$

$$\left.\begin{aligned}\vec{x}_1 &= \vec{x}_\alpha - \vec{a}_1\left(\vec{d}_\alpha\right) \\ \vec{x}_2 &= \vec{x}_\beta - \vec{a}_2\left(\vec{d}_\beta\right) \\ \vec{x}_3 &= \vec{x}_\gamma - \vec{a}_3\left(\vec{d}_\gamma\right)\end{aligned}\right\} \tag{24}$$

Using the below equation (Durairasan and Balasubramanian, 2020), the α, β, and γ mean value positions are found

$$\vec{x}(t+1) = \frac{\vec{x}_1 + \vec{x}_2 + \vec{x}_3}{3} \tag{25}$$

The procedure of the suggested approach is as follows:

Step 1: Create the populations.
Step 2: Using **Eqs 21**, **22**, calculate the values of Y, a, and Z.

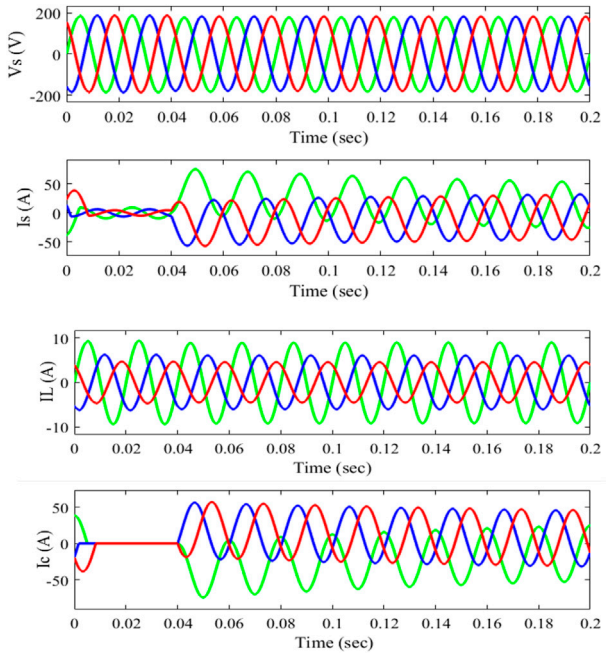

FIGURE 14 | With the passive filter for unbalanced load source voltage (V_s), source current (I_s), and load current (I_L).

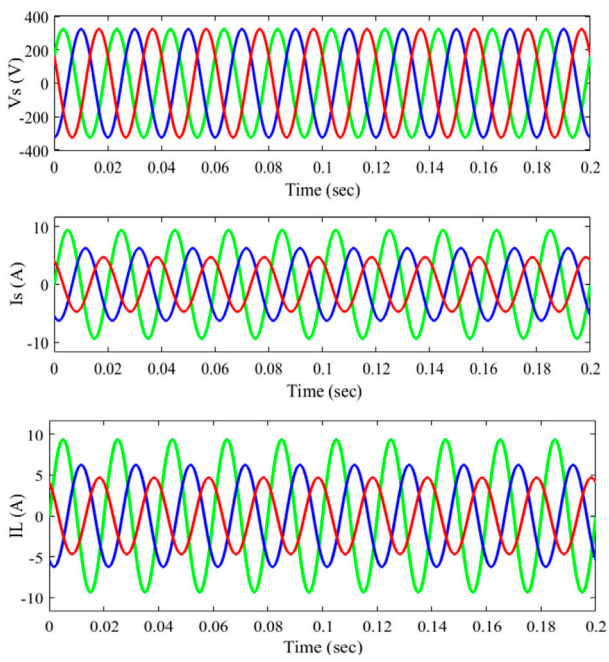

FIGURE 15 | Total harmonic distortion with the passive filter.

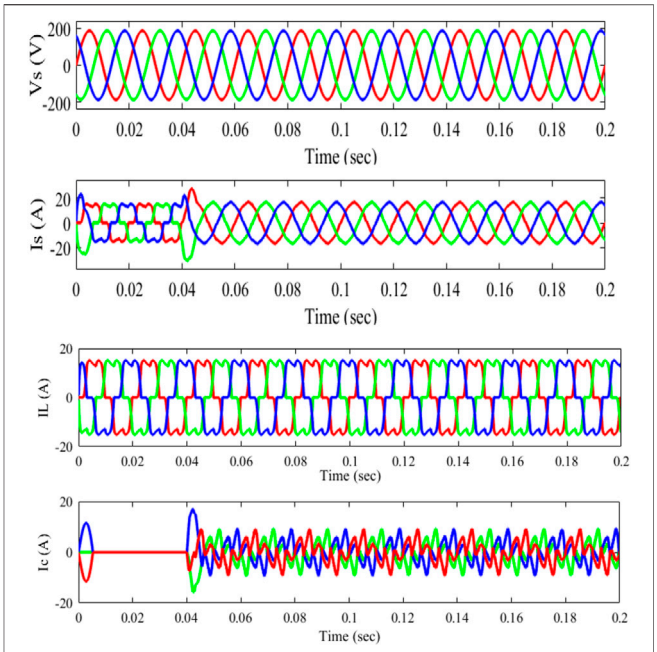

FIGURE 16 | With SHAPF for nonlinear load source voltage (V_s), source current (I_s), load current (I_L), and compensating current (I_c).

Step 3: A random location is created from the Search agent.
Step 4: The fitness values of Gray wolves are computed using an objective function.
Step 5: The position of the Gray wolves as well as the parameters A, a, and C, are changed.
Step 6: Using fitness calculations, the optimal option for the next generation is selected.
Step 7: x_α, x_β, and x_γ are all updated.
Step 8: If the halting condition is not met, the preceding steps are repeated.
Step 9: The controller's optimal settings are determined.

5.1 Fractional Order Proportional Integral Controller

The FOPI controller's transfer function is represented by the below equation (Goud et al., 2021a; Dashtdar et al., 2021b; Goud et al., 2021b; Goud et al., 2021c). The FOPI controller design is seen in **Figure 9**

$$U(t) = K_p e(t) + K_i \int_t^{\lambda} e(t) \tag{26}$$

The values of the controller depend on K_p, K_i, and fractional-order λ and are represented in **Table 3**.

6 SIMULATION RESULTS

HSHAPF performance is analyzed in MATLAB/Simulink. Two different loads are considered: nonlinear load and unbalanced load. Without the filter, the THD was 27.43%, and after HSHAPF

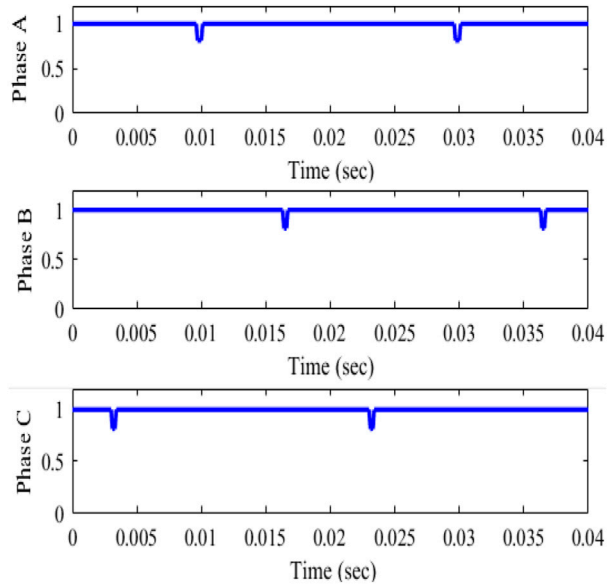

FIGURE 17 | Total harmonic distortion without the filter.

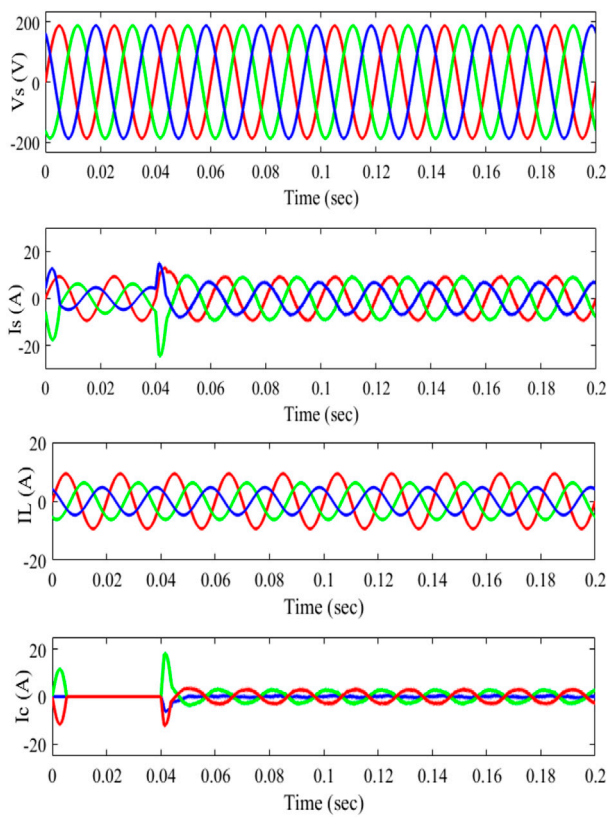

FIGURE 18 | Total harmonic distortion with GWO-based SHAPF.

with the GWO-based FOPI controller, the THD is reduced to 1.74%. Similarly, with a passive filter, the THD is 7.67%, and with APF with the PI controller, the THD is 5.85%.

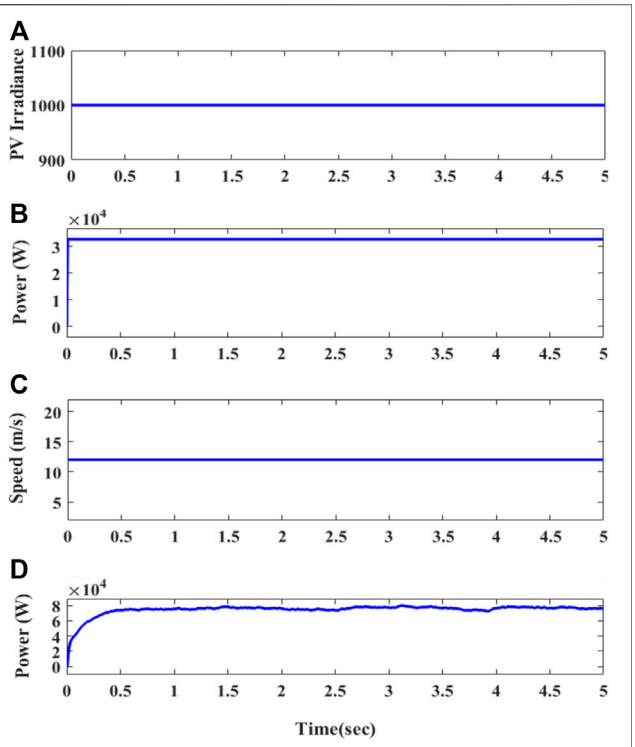

FIGURE 19 | Power factor for phases A, B, and C.

6.1 Case I: Without the Filter for Nonlinear Load

At PCC, nonlinear load is connected, which is generally time-varying and difficult to observe system dynamic performances. At the first diode, the rectifier load is connected to the PCC. During t = 0.01 s to t = 0.2 s, an additional RL segment is added. The figure shows that the inputs to PV and wind are 800–1000 w/m^2 and 12–15 m/s, respectively.

In this case, the system dynamic performance of the system without using the filter is analyzed. **Figure 10** shows that the harmonics are not eliminated. It represents the source voltage (Vs.), source current (I_s), and load current (I_L). During time intervals t = 0.01 s to t = 0.04 s, harmonics are observed in both the source current and load current when the design is employed without the filter. **Figure 8** represents the THD of about 27.43%. For the sudden change in load at the PCC, it is observed that the system has high dynamic performance.

6.2 Case II: Without the Filter for Unbalanced Load

Initially, the load connected at the PCC is the diode rectifier which is then replaced with a single-phase diode rectifier which behaves as an unbalanced load during t = 0.01 s and is removed at t = 0.2 s. From **Figure 11**, PCC voltage V_s, supply current I_s, and unbalanced current I_L show the dynamic performances of the system.

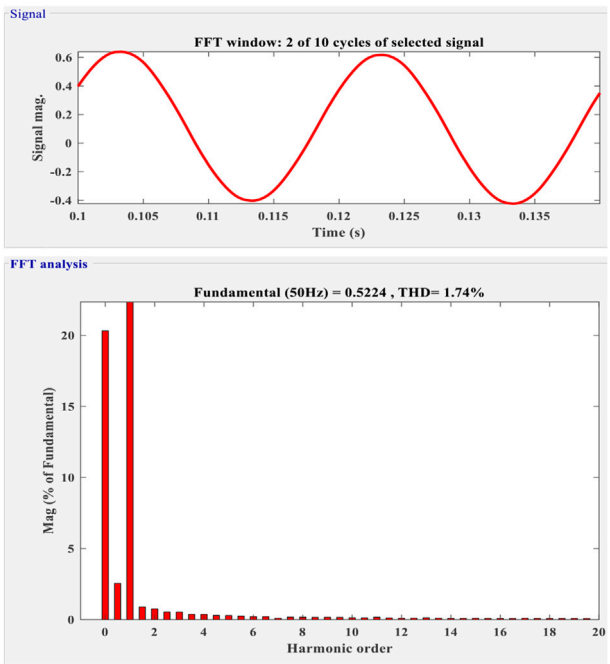

FIGURE 20 | With SHAPF for unbalanced linear load source voltage (V_s), source current (I_s), load current (I_L), and compensating current (I_c).

6.3 Case III: With the Passive Filter for Nonlinear Load

Sudden changes in loads are nonlinear, so it is important to analyze the system's dynamic characteristics. A diode rectifier load is first connected to the PCC. From t = 0.01 s to t = 0.04 s, an extra load of the RL circuit is added to the previous load. During the nonlinear load, the current decreases from 45A to 5A at time t = 0.01 s and then climbs from 5 to 45A at time t = 0.04 s. The voltage at PCC V_s, supply current I_s, variable load current I_L, and compensating current I_c between t = 0.01 s and t = 0.04 s are shown in **Figure 12**. The findings show that nonlinear control has high dynamic performance for fast-changing loads.

6.4 Case IV: With Passive Filter Unbalanced Load

The imbalance, harmonics, and reactive power of an unbalanced nonlinear load must be rectified at PCC. A three-phase diode is used as the load at first. At t = 0.01 s, a one-phase rectifier is connected in series to the PCC and removed at t = 0.04 s. The input values for PV are 1000 w/m^2 and a wind speed of 12 m/s, depicted in **Figure 13**. Between t = 0.01 s and t = 0.04 s, the PCC is connected to a resistor between phases a and b and then withdrawn. In **Figure 14**, V_s represents the PCC voltage, I_s represents the source current, I_L represents the current at load, and I_c represents the inverter. Even with erratic supply currents, PCC's source currents are balanced. As a consequence, the recommended control may be able to balance line currents while simultaneously correcting for reactive and harmonic components of a load. **Figure 15** shows that the THD is 7.67%, which is lowered by using a passive filter.

TABLE 4 | Comparison of THDs.

Total harmonic distortion	
Without the filter	27.43 (%)
With the passive filter	7.67
APF with PI controllers	5.85
With the GWO-FOPI controller	1.74

6.5 Case V: With the Shunt Active Power Filter for Nonlinear Load

Because rapid change loads are nonlinear, time-varying loads, it is critical to analyze the system's dynamic characteristics. The PCC is initially linked to a three-phase diode rectifier load. An extra load of the RL circuit is added to the current load from t = 4 s to t = 5 s. At time t = 0.01 s, the nonlinear load current rises from 45A to 5A, and at time t = 0.04 s, it climbs from 5 to 45A. **Figure 16** represents the voltage at PCC V_s, the supply current I_s, the variable load current IL, and the compensating current I_c between periods t = 0.01 s and t = 0.04 s. The findings show that nonlinear control has high dynamic performance for fast-changing loads. As the PCC load current increases, the THD value rises. The THD is 27.43%, depicted in **Figure 17** without the filter, 7.67% depicted in **Figure 15** with the passive filter, and 1.74% with the suggested GWO-FOPI controller with SHAPF depicted in **Figure 18**. The power factors for phases A, B, and C are all 0.99, as shown in **Figure 19**.

6.6 Case VI: With Hybrid Shunt Active Power Filter Unbalanced Load

The variations, reactive power, and harmonics of an unbalanced load must be rectified at PCC. In the beginning, a single-phase diode is used as the load. A single-phase rectifier is connected in series to the PCC at = 0.01 s. Between t = 0.01 s and t = 0.04 s, the PCC is connected to a resistor between phases a and b and then withdrawn. **Figure 20** represents the voltage at PCC V_s, the supply current I_s, the variable load current I_L, and the inverter current I_c. The supply current is balanced at PCC even during irregularities. As a consequence, the recommended control may be able to balance line currents while simultaneously correcting for reactive and harmonic load current components. **Table 4** compares THDs without a filter to THDs with a filter.

Finally, under the IEEE 519 standards, the suggested GWO-based FOPI controller with decreased THD is proposed. With the suggested controller, the THD is decreased by 1.74%.

7 CONCLUSION

PQ in a grid-connected hybrid system with the battery as an energy storing device is proposed with the GWO-based FOPI controller with SHAPF circuit to mitigate the issues. The optimal pulses required for the FOPI controller are attained with the GWO technique. This system has been considered in three different practices: without a filter, the THD is 27.43%; with a passive filter, the THD is 7.67%; the APF with the PI controller is 5.85%, and with the proposed GWO-FOPI controller, it resulted in 1.74% total harmonic reduction. The recommended method's simulation results are then validated in the MATLAB/Simulink software. The final results of the hybrid system proved the GWO controller's practicality and effectiveness in decreasing PQ concerns including THD.

DATA AVAILABILITY STATEMENT

The original contributions presented in the study are included in the article/supplementary material; further inquiries can be directed to the corresponding author.

AUTHOR CONTRIBUTIONS

All authors listed have made a substantial, direct, and intellectual contribution to the work and approved it for publication.

REFERENCES

Aljendy, R., Nasyrov, R. R., Abdelaziz, A. Y., and Diab, A. A. Z. (2019). Enhancement of Power Quality with Hybrid Distributed Generation and FACTS Device. *IETE J. Res.*, 1–12. doi:10.1080/03772063.2019.1698321

Amir, M., and Srivastava, S. K. (2019). "Analysis of Harmonic Distortion in PV-Wind-Battery Based Hybrid Renewable Energy System for Microgrid Development," in *Applications of Computing, Automation and Wireless Systems in Electrical Engineering* (Singapore: Springer), 1223–1231. doi:10.1007/978-981-13-6772-4_107

Arkhangelski, J., Roncero-Sánchez, P., Abdou-Tankari, M., Vázquez, J., and Lefebvre, G. (2019). Control and Restrictions of a Hybrid Renewable Energy System Connected to the Grid: A Battery and Supercapacitor Storage Case. *Energies* 12, 2776. doi:10.3390/en12142776

Bhupesh, N. K., Kotaiah Chowdary, K., and Subrahmanyam, V. (2019). Renewable Energy Hybrid Power System with Improvement of Power Quality in Grid by Using DVSI. *Renew. Energy* 6, 1300.

Dash, S. K., Ray, P. K., and Ray, P. K. (2018). Power Quality Improvement Utilizing PV Fed Unified Power Quality Conditioner Based on UV-PI and PR-R Controller. *Cpss Tpea* 3, 243–253. doi:10.24295/cpsstpea.2018.00024

Dashtdar, M., Bajaj, M., Hosseinimoghadam, S. M. S., Sami, I., Choudhury, S., Rehman, A. U., et al. (2021a). Improving Voltage Profile and Reducing Power Losses Based on Reconfiguration and Optimal Placement of UPQC in the Network by Considering System Reliability Indices. *Int. Trans. Electr. Energy Syst.* 31 (11), e13120. doi:10.1002/2050-7038.13120

Dashtdar, M., Nazir, M. S., Hosseinimoghadam, S. M. S., and Bajaj, M. (2021b). Improving the Sharing of Active and Reactive Power of the Islanded Microgrid Based on Load Voltage Control. *Smart Sci.* 10, 1–16. doi:10.1080/23080477.2021.2012010

Durairasan, M., and Balasubramanian, D. (2020). An Efficient Control Strategy for Optimal Power Flow Management from a Renewable Energy Source to a Generalized Three-phase Microgrid System: A Hybrid Squirrel Search Algorithm with Whale Optimization Algorithm Approach. *Trans. Inst. Meas. Control* 42, 1960–1976. doi:10.1177/0142331220901628

Goud, B. S., and Rao, B. L. (2021). Power Quality Enhancement in Grid-Connected PV/wind/battery Using UPQC: Atom Search Optimization. *J. Electr. Eng. Technol.* 16, 821–835. doi:10.1007/s42835-020-00644-x

Goud, B. S., and Rao, B. L. (2020). Power Quality Improvement in Hybrid Renewable Energy Source Grid-Connected System with Grey Wolf Optimization. *Int. J. Renew. Energy Res. (IJRER)* 10, 1264–1276. doi:10.20508/ijrer.v10i3.11318.g8004

Goud, B. S., Rao, B. L., Reddy, B. N., Rajesh, N., Anjan, B., and Reddy, C. R. (2020). "Optimization Techniques in PV-Wind Based Distribution Generation-A Brief Review," in 2020 IEEE 17th India Council International Conference (INDICON), India, 10-13 Dec. 2020, 1–6.

Goud, B. S., Rao, B. L., and Reddy, C. R. (2021a). An Intelligent Technique for Optimal Power Quality Reinforcement in a Grid-connected HRES System: EVORFA Technique. *Int. J. Numer. Model. Electron. Netw. Devices Fields* 34, e2833. doi:10.1002/jnm.2833

Goud, B. S., Reddy, C. R., Bajaj, M., Elattar, E. E., and Kamel, S. (2021b). Power Quality Improvement Using Distributed Power Flow Controller with BWO-Based FOPID Controller. *Sustainability* 13, 11194. doi:10.3390/su132011194

Goud, B. S., and Reddy, C. R. (2020). Essentials for Grid Integration of Hybrid Renewable Energy Systems: a Brief Review. *Int. J. Renew. Energy Res. (IJRER)* 10, 813–830. doi:10.20508/ijrer.v10i2.10772.g7950

Goud, B. S., Reddy, C. R., Rakesh, T., Rajesh, N., Reddy, B. N., and Aymen, F. (2021c). Grid Integration of Renewable Energy Sources Using GA Technique for Improving Power Quality. *Int. J. Renew. Energy Res. (IJRER)* 11 (3), 1390–1402. doi:10.20508/ijrer.v11i3.12292.g8283

Hari Prabhu, M., and Sundararaju, K. (2020). Power Quality Improvement of Solar Power Plants in Grid Connected System Using Novel Resilient Direct Unbalanced Control (RDUC) Technique. *Microprocess. Microsystems* 75, 103016. doi:10.1016/j.micpro.2020.103016

Hussain, J., Hussain, M., Raza, S., and Siddique, M. (2019). Power Quality Improvement of Grid Connected Wind Energy System Using DSTATCOM-BESS. *Int. J. Renew. Energy Res.* 9, 1388–1397. doi:10.20508/ijrer.v9i3.9802.g7717

Imam, A. A., Sreerama Kumar, R., and Al-Turki, Y. A. (2020). Modeling and Simulation of a PI Controlled Shunt Active Power Filter for Power Quality Enhancement Based on P-Q Theory. *Electronics* 9 (4), 637. doi:10.3390/electronics9040637

Jamil, E., Hameed, S., Jamil, B., and Qurratulain (2019). Power Quality Improvement of Distribution System with Photovoltaic and Permanent Magnet Synchronous Generator Based Renewable Energy Farm Using Static Synchronous Compensator. *Sustain. Energy Technol. Assessments* 35, 98–116. doi:10.1016/j.seta.2019.06.006

Kuchibhatla, S. M., Padmavathi, D., and Rao, R. S. (2020). An Elephant Herding Optimization Algorithm-Based Static Switched Filter Compensation Scheme for Power Quality Improvement in Smart Grid. *J. Circuit Syst. Comp.* 29, 2050066. doi:10.1142/s0218126620500668

Meral, M. E., and Celik, D. (2018). DSOGI-PLL Based Power Control Method to Mitigate Control Errors under Disturbances of Grid Connected Hybrid Renewable Power Systems. *Adv. Electr. Electron. Eng.* 16, 81–91. doi:10.15598/aeee.v16i1.2485

Mohamed, Y. A.-R. I., and El-Saadany, E. F. (2009). A Control Method of Grid-Connected PWM Voltage Source Inverters to Mitigate Fast Voltage Disturbances. *IEEE Trans. Power Syst.* 24 (1), 489–491. doi:10.1109/tpwrs.2008.2006996

Mosobi, R. W., Chichi, T., and Gao, S. (2015). Power Quality Analysis of Hybrid Renewable Energy System. *Cogent Eng.* 2, 1005000. doi:10.1080/23311916.2015.1005000

Muthukumar, R., and Balamurugan, P. (2019). A Model Predictive Controller for Improvement in Power Quality from a Hybrid Renewable Energy System. *Soft Comput.* 23, 2627–2635. doi:10.1007/s00500-018-3626-7

Naresh, M., Soni, U. K., and ripathi, R. K. (2018). Power Flow Control and Power Quality Improvement in DFIG Based Wind Energy Conversion System Using Neuro Fuzzy System. *Int. J. Appl. Eng. Res.* 13, 5236–5243.

Pang, M., Shi, Y., Wang, W., and Pang, S. (2019). Optimal Sizing and Control of Hybrid Energy Storage System for Wind Power Using Hybrid Parallel PSO-GA Algorithm. *Energy Explor. Exploitation* 37, 558–578. doi:10.1177/0144598718784036

Rahmani, S., Mendalek, N., and Al-Haddad, K. (2010). Experimental Design of a Nonlinear Control Technique for Three-phase Shunt Active Power Filter.

IEEE Trans. Ind. Electron. 57 (10), 3364–3375. doi:10.1109/tie.2009.2038945

Rambabu, E., Praveena, E., and Kishore, P. V. (2011). Mitigation of Harmonics in Distribution System Using D-STATCOM. *Int. J. Sci. Eng. Res. IJSER* 2, 1–5.

Ravinder, K., and Bansal, H. O. (2019). Investigations on Shunt Active Power Filter in a PV-Wind-FC Based Hybrid Renewable Energy System to Improve Power Quality Using Hardware-In-The-Loop Testing Platform. *Electr. Power Syst. Res.* 177, 105957. doi:10.1016/j.epsr.2019.105957

Reddy, C. R., Goud, B. S., Aymen, F., Rao, G. S., and Bortoni, E. C. (2021). Power Quality Improvement in HRES Grid Connected System with FOPID Based Atom Search Optimization Technique. *Energies* 14 (18), 5812. doi:10.3390/en14185812

Sharaf, A. M., Wang, W., and Altas, I. H. (2010). A Novel Hybrid Active Filter Compensator for Stabilization of Wind-Utility Grid Interface Scheme. *Euro. Trans. Electr. Power* 20 (3), 306–326. doi:10.1002/etep.313

Sureshkumar, K., and Ponnusamy, V. (2020). Hybrid Renewable Energy Systems for Power Flow Management in Smart Grid Using an Efficient Hybrid Technique. *Trans. Inst. Meas. Control* 42, 2068–2087. doi:10.1177/0142331220904818

Conflict of Interest: The authors declare that the research was conducted in the absence of any commercial or financial relationships that could be construed as a potential conflict of interest.

Publisher's Note: All claims expressed in this article are solely those of the authors and do not necessarily represent those of their affiliated organizations or those of the publisher, the editors, and the reviewers. Any product that may be evaluated in this article or claim that may be made by its manufacturer is not guaranteed or endorsed by the publisher.